Probing Local Environments in Paramagnetic Europium−Substituted Keggin Solids by 31 P Magic Angle Spinning NMR Spectroscopy

ARTICLE *in* THE JOURNAL OF PHYSICAL CHEMISTRY B · JULY 2006

Impact Factor: 3.3 · DOI: 10.1021/jp061990z · Source: PubMed

7 AUTHORS, INCLUDING:

Tatyana Polenova
University of Delaware
88 PUBLICATIONS **1,760** CITATIONS

SEE PROFILE

Probing Local Environments in Paramagnetic Europium-Substituted Keggin Solids by ^{31}P Magic Angle Spinning NMR Spectroscopy

Wenlin Huang,[†] Mark Schopfer,[†] Cheng Zhang,[‡] Robertha C. Howell,[‡] Becky A. Gee,[§] Lynn C. Francesconi,*[,‡] and Tatyana Polenova*[,†]

Department of Chemistry and Biochemistry, University of Delaware, Newark, Delaware 19716, Department of Chemistry, City University of New York—Hunter College, 695 Park Avenue, New York, New York 10021, and Department of Chemistry and Biochemistry, Long Island University—Brooklyn Campus, 1 University Plaza, Brooklyn, New York 11201

Received: March 30, 2006; In Final Form: May 6, 2006

Paramagnetic Eu-substituted Keggin oxopolytungstates crystallize in different forms, determined by the nature of the counterions. The crystal packing is in turn responsible for the variations in the geometry of paramagnetic Eu sites with respect to the anion core. We probed the paramagnetic environments in a series of Eu-substituted Keggin solids, by ^{31}P magic angle spinning NMR spectroscopy. ^{31}P spinning sideband envelopes are dominated by the electron−nuclear dipolar interaction. For the compounds under investigation, both the magnitude and the asymmetry parameter of the electron−nuclear dipolar coupling tensor are sensitive to the mutual arrangements of paramagnetic Eu sites in the crystal lattice. and also report on the stoichiometry of the anion. The electron−nuclear dipolar coupling tensors were calculated from the crystallographic coordinates and the experimentally determined effective magnetic moments, assuming a point dipole approximation. The computed tensors are in very good agreement with the experimental spectra. Furthermore, the P−Eu distance estimates, accurate to within 0.06−0.12 Å, can be obtained directly from the magnitude of the electron−nuclear dipolar coupling. This work demonstrates that ^{31}P MAS NMR spectroscopy is a useful probe for investigating local environments in paramagnetic Keggin solids.

Introduction

The Keggin-type oxoanions are the most investigated family of polyoxometalates.[1,2] Polyoxomolybdates $[PMo_{12}O_{40}]^{3-}$ have been known since 1826,[3,4] and the first structure of a related polyoxotungstate $[PW_{12}O_{40}]^{3-}$ was reported by Keggin in 1933.[5] Interest in Keggin polyoxometalates has been growing in the recent years.[1,2] Relatively facile functionalization of the oxoanion core $[PM_{12}O_{40}]^{3-}$, for example, via substituting different transition metals or rare earths metals (e.g., V(V), Cu(II), Ln(III), Eu(III)) into one or more of the framework metal sites allows for great versatility in the electronic, photochemical, magnetic, and catalytic properties of Keggin compounds, making them attractive for the design of new materials for a variety of applications.[2,6,7]

Luminescent rare earth complexes have found a variety of applications as electroluminescent optical devices and probes, lasers, and luminophores for displays.[8,9] Lanthanide-substituted polyoxometalates are becoming of special interest because of their excellent luminescent characteristics and the possibility to fine-tune their electronic properties via synthesis of mixed-addenda anions or use of different countercations.[10−13] Fluorescent and luminescent polyoxometalate materials are typically fabricated as thin solid films of hybrid organic/inorganic materials.[11−18]

It has been recently demonstrated that luminescence properties of thin polyoxometalate films differ from those of the bulk solids.[18] An interaction between the polyoxoanion and the organic matrix leading to the altered site symmetry of the rare earth atom in the polyoxometalate has been proposed on the basis of the bulk changes detected in the excitation and emission spectra. However, no further details are available from these measurements, owing to the intrinsic lack of site resolution. Clearly, to exploit variations in the site symmetry for potential fine-tuning the luminescent properties of these materials, the local geometry of the rare earths sites in thin films needs to be thoroughly characterized, and therefore site-specific structural probes are required.

A large number of polyoxometalate materials with favorable luminescent characteristics contain rare earth elements in their paramagnetic states, where the rare earth atoms are typically responsible for the luminescence.[19,20] At the same time, paramagnetism of these atoms can be conveniently exploited as a site-specific probe of local structure in polyoxometalate solids, for example in solid-state NMR spectroscopic measurements of the dipolar interaction between the unpaired electron and an NMR active nucleus in proximity to the paramagnetic center.

In this study, we addressed the local environments of the paramagnetic Eu(III) sites in Keggin polyoxometalates, by ^{31}P magic angle spinning NMR spectroscopy. It has been discussed previously that various nuclear probes (e.g., ^{13}C, ^{1}H, ^{2}H, ^{6}Li, ^{7}Li, ^{31}P) report on the local paramagnetic environments in inorganic solids.[21−29] Anisotropic dipolar coupling between the electronic and the nuclear magnetic moments is often the

* To whom correspondence should be addressed. (T.P.) E-mail: tpolenov@chem.udel.edu. Tel: (302) 831-1968. Fax: (302) 831-6335. (L.C.F) E-mail: lfrances@hunter.cuny.edu. Tel: (212) 772-5353. Fax: (212) 772-5332.

[†] University of Delaware.

[‡] City University of New York-Hunter College.

[§] Long Island University-Brooklyn Campus.

10.1021/jp061990z CCC: $33.50
Published on Web 06/08/2006

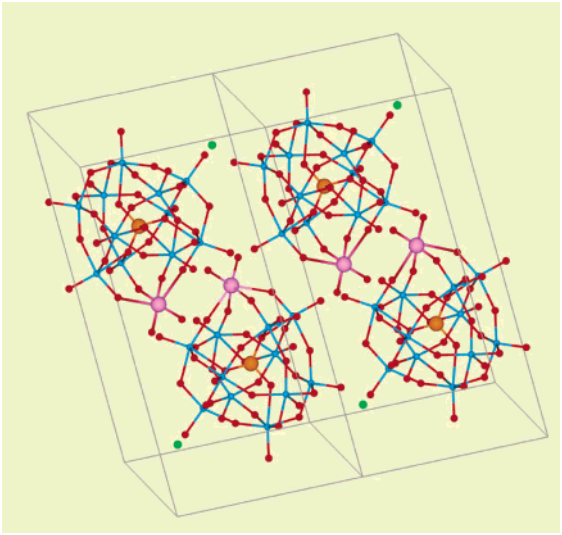

Figure 1. Coordination environments and unit cell of monomeric Al(H$_3$O){Eu(H$_2$O)$_2$PW$_{11}$O$_{34}$}·20H$_2$O (**3**).[32] View down the crystallographic *b* axis to indicate the geometry of paramagnetic Eu^{3+} centers. The anion is shown in a ball-and-stick representation. Atoms shown are W (blue), O (red), P (orange), Eu (pink), and Al (green). Water molecules are omitted for clarity.

dominant interaction in paramagnetic solids. It gives rise to large asymmetric spinning sideband manifolds in the MAS spectra and bears information about the local geometry of the paramagnetic sites with respect to the nucleus of interest. This geometric information can be extracted by simulations of the MAS spectra.

We investigated a series of five Eu-substituted paramagnetic polyoxoanions prepared as salts of different countercations, plus two diamagnetic vanadium-substituted compounds. We demonstrate that the spinning sideband envelopes as well as the isotropic chemical shifts are very sensitive to the local geometry of the paramagnetic centers. The spinning sideband patterns calculated from the X-ray crystallographic coordinates using experimentally determined effective magnetic moments and following a point dipole approximation, agree with the experimental spectra to within 1−6%. Furthermore, we show that P−Eu distances can be estimated to within 0.06−0.12 Å using an isolated spin-pair model and without the a priori knowledge of the X-ray structure. Overall, the results suggest that ^{31}P magic spinning NMR spectroscopy is a quick and sensitive probe of local geometry in paramagnetic Keggin polyoxometalates and may be particularly useful in the absence of long-range order.

Experimental Section

Materials and Syntheses. All chemicals were obtained from Aldrich and used without further purification: sodium tungstate dihydrate (Na$_2$WO$_4$·2H$_2$O), tungstophosphoric acid (H$_3$PW$_{12}$O$_{40}$·*x*H$_2$O), vanadyl sulfate (VOSO$_4$), sodium metavanadate (NaVO$_3$), sulfuric acid, cesium chloride, hydrochloric acid, glacial acetic acid.

K$_7$PW$_{11}$O$_{39}$ was isolated as a K$^+$ salt from H$_3$PW$_{12}$O$_{40}$ via treatment with KOH and subsequent addition of KCl.[30]

K$_4$PVW$_{11}$O$_{40}$ (**1**), 1,2-K$_5$[PV$_2$W$_{10}$O$_{40}$] (**2**), Al(H$_3$O){Eu(H$_2$O)$_2$PW$_{11}$O$_{34}$}·20H$_2$O (**3**), Cs$_{11}$[Eu(PW$_{11}$O$_{34}$)$_2$]·28H$_2$O (**6**), and (NH$_4$)$_{22}$[(Eu$_2$PW$_{10}$O$_{38}$)$_4$(W$_3$O$_8$(H$_2$O)$_2$(OH)$_4$)]·44H$_2$O (**7**), were synthesized according to the previously reported protocols.[30,31] Compounds **1**−**3**, **6**, and **7** have been crystallographically characterized.[30,32] Coordination environments and units cells of **3**, **6**, and **7** are illustrated in Figures 1, 2, and 3, respectively.

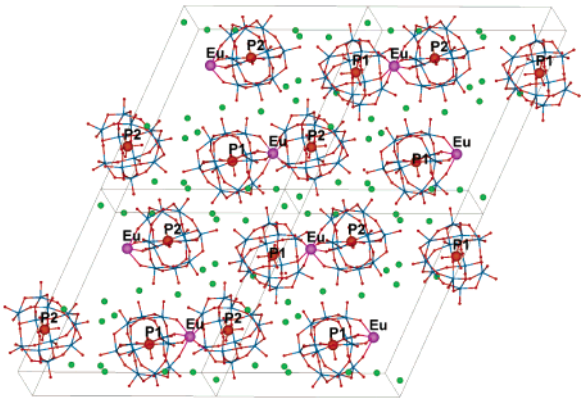

Figure 2. Coordination environments and unit cell of dimeric Cs$_{11}$Eu(PW$_{11}$O$_{34}$)$_2$·28H$_2$O (**6**).[32] View down the crystallographic *a* axis to indicate the geometry of paramagnetic Eu^{3+} centers. The anion is shown in a ball-and-stick representation. Atoms shown are W (blue), O (red), P (orange), Eu (pink), and Al (green). Water molecules are omitted for clarity. The designation of the two crystallographically inequivalent phosphorus atoms as P1 and P2 is arbitrary.

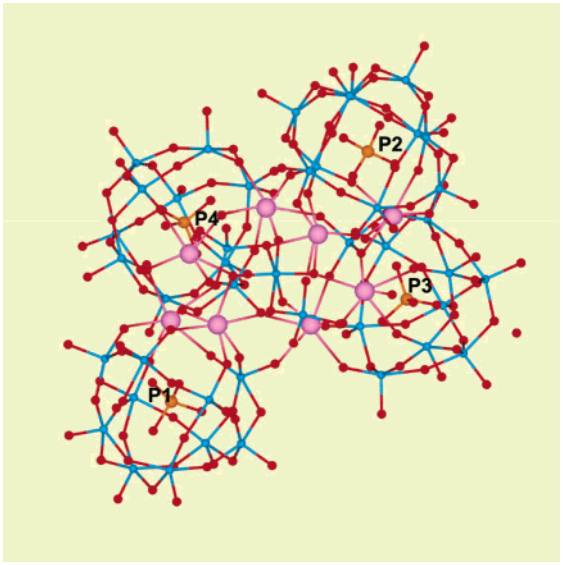

Figure 3. Coordination environment of tetrameric (NH$_4$)$_{22}${(Eu$_2$PW$_{10}$O$_{38}$)$_4$(W$_3$O$_8$(H$_2$O)$_2$(OH)$_4$)}·44H$_2$O (**7**).[32] Countercation molecules are omitted for clarity. The designation of the four crystallographically inequivalent phosphorus atoms as P1, P2, P3, and P4 is arbitrary.

For solid-state NMR measurements, the crystalline forms of **6** and **7** were used, while a fresh batch of **3** was synthesized. The identity of **3** was corroborated by its solution NMR isotropic chemical shifts (Table 1), which are in agreement with the previously reported values.[30]

For synthesis of K[Eu (PW$_{11}$O$_{39}$)$_2$]$^{13-}$ (**4**), 3 g of K$_7$PW$_{11}$O$_{39}$ was dissolved in 10 mL of distilled H$_2$O at room temperature and added dropwise to 10 mL of 0.4 M aqueous solution of EuCl$_3$·6H$_2$O. The resulting solution was stirred vigorously for a few minutes, followed by the addition of KCl (0.80 g, 10.07 mmol) and 80 mL of EtOH. A white precipitate was collected by filtration and dried under suction, ^{31}P solution NMR shows the formation of a 1:2 K[Eu (PW$_{11}$O$_{39}$)$_2$]$^{13-}$ complex.[30]

For synthesis of Li$_4$[Eu(H$_2$O)$_2$PW$_{11}$O$_{34}$] (**5**), 6.09 g of K$_7$PW$_{11}$O$_{39}$ was dissolved in 25 mL of distilled H$_2$O at 40 °C and was added dropwise to 10 mL of 0.2 M aqueous solution of EuCl$_3$·6H$_2$O. The resulting solution was stirred vigorously for a few minutes, followed by the addition of LiCl (0.87 g, 20.47 mmol) and 105 mL of EtOH. A white precipitate was collected

TABLE 1: Experimental ^{31}P Solid-State and Solution NMR Parameters for the Vanadium and Europium-Substituted Keggin Oxotungstates 1−7[a]: ^{31}P Isotropic Chemical Shifts (δ_{iso}), Combined Electron−Nuclear Dipolar and Chemical Shielding Anisotropies ($\Delta\delta$, η), T_1 Spin−Lattice and T_2 Spin−Spin Relaxation Parameters at $T = 293$ K

compd	$\Delta\delta$, ppm[c]	η[c]	δ_{iso}, ppm ($\Delta\delta_{iso}$),[d] ppm	δ_{iso}, ppm (soln)	T_1 (s)	T_2 (s)
1[b]	16.0 ± 1.4	0.9 ± 0.1	7.6 (0)		22.9	0.132
2[b]	13.0 ± 3.0	0.9 ± 0.1	7.0 (0)		35.9	0.045
3	161.5 ± 4.4	0.6 ± 0.08	5.6 (−2)	4.965 (pH = 5) 5.035 (pH = 2−3)		
4	153.0 ± 0.9	0.12 ± 0.03	19.5 (11.9)		2.1	0.016
5	170.7 ± 1.8	0.22 ± 0.15	27.4 (19.8)		2.5	0.016
6	154.0 ± 1.0	0.14 ± 0.07	20.0 (12.4)		3.5	0.027
7	P1: 313.1 ± 3.7 P2: 302.8 ± 6.3 P3: 297.9 ± 5.2 P4: 287.4 ± 6.3	P1: 0.39 ± 0.03 P2: 0.52 ± 0.01 P3: 0.28 ± 0.08 P4: 0.52 ± 0.06	P1: 48.2 (40.6) P2: 54.2 (46.6) P3: 37.3 (29.7) P4: 39.7 (32.1)		1.7	0.016

[a] Data are shown for $K_4PVW_{11}O_{40}$ (**1**), 1,2-$K_5[PV_2W_{10}O_{40}]$ (**2**), $Al(H_3O)\{Eu(H_2O)_2PW_{11}O_{34}\}\cdot 20H_2O$ (**3**), $K[EuPW_{11}O_{40}]$ (**4**), $Li_4[Eu(H_2O)_2PW_{11}O_{34}]$ (**5**), $Cs_{11}[Eu(PW_{11}O_{34})_2]\cdot 28H_2O$ (**6**), and $(NH_4)_{22}[(Eu_2PW_{10}O_{38})_4(W_3O_8(H_2O)_2(OH)_4)]\cdot 44H_2O$ (**7**) [b] For the diamagnetic Keggin solids I and II, $\Delta\delta$ and η are chemical-shielding anisotropies. [c] These are values obtained by averaging the experimental parameters extracted from the spectra acquired at several different spinning frequencies. Mean values and standard errors are reported. [d] Apparent paramagnetic shifts.

by filtration and dried under suction. ^{31}P solution NMR shows the formation of a 1:1 $[Eu(PW_{11}O_{39})]^{4-}$ complex.[30]

Solid-State NMR Spectroscopy. ^{31}P solid-state NMR spectra were acquired at 162.028 MHz (9.4 T) on a Tecmag Discovery spectrometer using a 4 mm Varian T3 probe. Spectra were recorded using 8−16 mg of sample. The magic angle was adjusted using $NaNO_3$ (by detecting the ^{23}Na MAS signal). For each of the compounds, spectra at several different spinning frequencies ranging between 3 and 15 kHz were acquired. A single 3 μs pulse ($\gamma H_1/2\pi = 83.3$ kHz) was employed; pulse delays of 1 s and 5−10 s were used for paramagnetic compounds **3**−**7**, and for the diamagnetic compounds **1**−**2**, respectively. The MAS spinning frequency was controlled to within ±2 Hz. A total of 1024 complex data points were acquired. T_1 and T_2 relaxation parameters were measured using the inversion−recovery[33] and Carr−Purcell−Meiboom−Gill[34] pulse sequences. For each T_1 and T_2 curve, 16 data points were acquired. The spectra were fit to a single-exponential function. The data were processed by Fourier transformation and baseline correction using the MestRe−C23 NMR data processing software.[35] Isotropic chemical shifts are reported with respect to the 85% H_3PO_4 used as an external reference.

Determination of Effective Magnetic Moments. Field dependent magnetic moment measurements for **5** and **7** (ca. 45 to 9900 Oe) were performed at approximately 21 °C on a LakeShore 7300 vibrating sample magnetometer. Powdered samples were carefully weighed and packed in polychlorotrifluoroethylene (Kel-F) sample holders. Corrections for the diamagnetic contribution from the Kel-F sample holder were made by measurement of the field dependent magnetic moment of the empty sample holders. Closed shell diamagnetic contributions to the measured magnetic moments were obtained from the literature.[36]

Simulations of the NMR Spectra. Numerical simulations of the experimental ^{31}P solid-state NMR spectra were performed on a 1.1 GHz Pentium-4 PC under the Linux environment using the Simpson software package.[37] The independent parameters describing the CSA tensor anisotropies and calculations of the shielding tensors were also performed using the Herzfeld-Berger algorithm[38] implemented in the HBA 1.4.4 program.[39]

Calculation of Electron−Nuclear Dipolar Coupling Tensors. ^{31}P MAS NMR spectra of paramagnetic solids are dominated by the electron−nuclear dipolar interaction.[22,25] The total Hamiltonian for a spin-$^1/_2$ nucleus in a paramagnetic system is

$$H = H_{Zeeman} + H_{RF} + H_{DIP}^{paramagn} + H_{CSA} + H_{FC} + H_{DIP} \quad (1)$$

The terms in the Hamiltonian represent the Zeeman, the radio frequency field, the electron−nuclear dipolar interaction, the chemical-shielding anisotropy, the Fermi contact shift, and the dipolar interaction between two nuclei. The dominant term in the interaction part of the Hamiltonian is the electron−nuclear anisotropic dipolar coupling. In this work, we are making several assumptions: (1) The anisotropic part of the Fermi contact shift and the dipolar interaction between two nuclei are smaller than the paramagnetic dipolar and the chemical-shielding anisotropy terms. (2) The point-dipole approximation is valid for the description of electronic-nuclear dipolar coupling. (3) The electron−nuclear interaction is described as a second rank tensor, that is, the g anisotropy is neglected.

The electron−nuclear dipolar coupling and the chemical-shielding anisotropy can be expressed as follows:

$$H_{DIP}^{paramagn} = \frac{\mu_0}{4\pi}\bar{\mu}_e\cdot\tilde{D}_{en}\cdot\bar{\mu}_n \quad (2)$$

$$H_{CSA} = \gamma\tilde{\sigma}\cdot B_0\cdot I_z \quad (3)$$

where γ is the gyromagnetic ratio of the nucleus, $\tilde{\sigma}$ is the chemical-shielding anisotropy tensor, B_0 is the Larmor frequency of the nucleus, I_z is the z component of the nuclear spin operator, μ_0 is the magnetic permeability, $\bar{\mu}_e$ is the thermally averaged electronic magnetic moment, $\tilde{D}_{en}$ is the electron−nuclear dipolar coupling tensor, and $\bar{\mu}_n$ is the nuclear magnetic moment.

If paramagnetism arises solely from the spin component, the thermally averaged electronic magnetic moment can be defined as follows:

$$\bar{\mu}_e = \frac{{\mu_B}^2 S(S+1)}{3k_B T}\cdot\tilde{g}\cdot\tilde{g}\cdot H_0 \quad (4)$$

where μ_B is the Bohr magneton, S is the electron spin quantum number, k_B is the Boltzmann's constant, $\tilde{g}$ is the electron g-tensor, and H_0 is the magnetic field strength. For rare earth elements, large spin−orbit coupling is present, and the spin-only formula is not valid.[40] For an accurate description of rare

earth solids, the effective magnetic moments have to be experimentally determined.

$\tilde{D}_{en}$ is expressed in a matrix representation:[22]

$$\tilde{D}_{en} = \frac{1}{r^3}(\delta_{\alpha\beta} - 3e_\alpha e_\beta) \quad (5)$$

where r is the electron−nuclear distance, δ is the Kronecker delta, e_α and e_β are the (x, y, z) components of the dipolar vector connecting the electron and the nucleus and assuming a point-dipole approximation.

In Keggin solids addressed in this study, electronic-nuclear dipolar coupling matrices arising from the interactions of ^{31}P with multiple Eu sites have to be considered. It has been stated previously,[21,22] that to a good approximation the local fields on the nucleus are independent contributions of the individual electrons. Thus the total electron−nuclear dipolar Hamiltonian can be obtained by summing up the dipolar matrices corresponding to the individual electron−nuclear spin pairs:

$$H_{DIP}^{paramagn} = \frac{\mu_0}{4\pi}\bar{\mu}_e\cdot(\sum_i \tilde{D}_{en,i})\cdot\mu_n \quad (6)$$

The final dipolar coupling tensor is transformed to its principal axes system by diagonalization of the corresponding matrix, to obtain its eigenvalues δ_{xx}, δ_{yy}, δ_{zz}, and by convention $|\delta_{zz} - \delta_{iso}| \geq |\delta_{xx} - \delta_{iso}| \geq |\delta_{yy} - \delta_{iso}|$. The principal components are subsequently defined as

$$\Delta\delta = \delta_{zz} - \frac{1}{2}(\delta_{xx} + \delta_{yy}); \quad \eta = \frac{\delta_{yy} - \delta_{xx}}{\delta_{zz} - \delta_{iso}} \quad (7)$$

where $\Delta\delta$ is the electron−nuclear dipolar anisotropy determining the breadth of the dipolar coupling tensor and η is the asymmetry parameter of the dipolar coupling tensor characterizing the deviation of the dipolar tensor from the axial symmetry. Note that the electron−nuclear dipolar interaction does not result in first-order shifts of the resonance frequency.

The isotropic chemical shift δ_{iso} in the presence of the paramagnetic centers contains the contributions of the diamagnetic CSA and the Fermi contact interactions.

It is worth noting that the symmetry of the dipolar coupling between the nuclear and thermally averaged electronic magnetic moments resembles that of the chemical-shielding anisotropy interaction.[22] Therefore, the magic angle spinning spectra of spin-$^1/_2$ nuclei dipolar coupled to the unpaired electrons in paramagnetic centers can be numerically simulated using the Maricq and Waugh or Herzfeld and Berger algorithms.[38, 41]

The dipolar coupling tensors between the phosphorus atom and the paramagnetic nuclei in **3**−**7** were calculated as described above, using a home-written program in Mathematica 5.0 (Wolfram, Inc.). The experimental crystallographic coordinates and effective magnetic moments were utilized.

Results and Discussion

Stoichiometry and Structure of Keggin Solids Under Investigation. All of the compounds possess a substituted Keggin structure $(PW_{12}O_{40})^{6-}$, where the heteroatom is phosphorus. Vanadium is mono- and di-substituted in compounds $K_4PVW_{11}O_{40}$ (**1**), and 1,2-$K_5[PV_2W_{10}O_{40}]$ (**2**). Compounds (**3**) $(Al(H_3O)\{Eu(H_2O)_2PW_{11}O_{34}\}\cdot 20H_2O)$ and (**5**) $(Li_4[Eu(H_2O)_2PW_{11}O_{34}])$ are 1:1 $Eu/PW_{11}O_{39}^{7-}$ species wherein one Eu(III) is complexed to four oxygen atoms of one lacunary $PW_{11}O_{39}^{7-}$ ion. The crystal structure of **3** shows that other sites are complexed by water molecules and by a terminal W═O of an adjacent $PW_{11}O_{39}^{7-}$ ion. While we do not have a crystal structure of **5**, and therefore, cannot specify the number of Li^+ countercations, the solution NMR clearly shows the 1:1 nature of the complex. Therefore, we denote **5** as $Li[Eu\ PW_{11}O_{39}]^{4-}$ to reflect the 1:1 formulation and the Li^+ salt. Compound (**4**) $K[Eu\ (PW_{11}O_{39})_2]^{13-}$ and compound (**6**) $Cs_{11}[Eu(PW_{11}O_{34})_2]\cdot 28H_2O$ are 1:2 $Eu/PW_{11}O_{39}^{7-}$ species wherein one Eu(III) is complexed to the four oxygen atoms of each of 2 lacunary $PW_{11}O_{39}^{7-}$ ions. The solution ^{31}P NMR clearly shows that **4** is a 1:2 species. Since we do not have an X-ray structure, we cannot specify the number of K^+ ions. We denote this complex as $K[Eu\ (PW_{11}O_{39})_2]^{13-}$ to reflect the 1:2 formulation as a K^+ salt. The monomer formulation for **5** and the dimer formulation for **4** are consistent with our finding that Li^+ ions promote the formation of 1:1 Ln/polyoxometalate species, while K^+ and Cs^+ promote the formation of 1:2 lanthanide/polyoxometalate species.[30,42,43] Compound (**7**) $(NH_4)_{22}[(Eu_2PW_{10}O_{38})_4(W_3O_8(H_2O)_2(OH)_4)]\cdot 44H_2O$ is an assembly of four divacant Keggin fragments tied together by eight Eu(III) ions with two Eu(III) ions substituted for two W═O units in each of the four divacant Keggin ions.

Effective Magnetic Moments of $Li_4[Eu(H_2O)_2PW_{11}O_{34}]$ (5) and $(NH_4)_{22}[(Eu_2PW_{10}O_{38})_4(W_3O_8(H_2O)_2(OH)_4)]\cdot 44H_2O$ (7). Effective magnetic moments of **5** and **7** are 3.13 and 3.37 μ_B at 294 K, respectively. These values are lower than the effective magnetic moments of the Eu^{3+} ion in $Eu_2(SO_4)_3$, which were experimentally determined to range between 3.41 and 3.61 μ_B at 293 K depending on the hydration level of the salt.[44−46] As already seen in many previous reports, the magnetic moments for europium-containing compounds are not in good agreement with the theoretical predictions for the free Eu^{3+} ion,[44] and therefore the knowledge of the experimental moments is important for analysis of the electron−nuclear dipolar interaction from the ^{31}P MAS NMR spectra. Using the effective magnetic moments of the free Eu^{3+} ion may result in 10−15% errors in the calculated electron−nuclear dipolar anisotropies. In our work, we assumed that the magnetic moments of monomeric and dimeric compounds **3**, **4**, and **6** will be very similar to that of **5**.

^{31}P MAS NMR Spectra of Diamagnetic and Paramagnetic Keggin Solids. The ^{31}P MAS solid-state NMR spectra of the Keggin compounds **1**−**7** are presented in Figure 4. The isotropic chemical shifts are compiled in Table 1. The diamagnetic solids $K_4PVW_{11}O_{40}$ (**1**) and 1,2-$K_5[PV_2W_{10}O_{40}]$ (**2**) give rise to a single peak in the MAS spectra, indicating that their chemical shift anisotropies are much smaller than the MAS rotation frequency of 5 kHz. As expected, the isotropic chemical shifts for these two Keggin solids are very similar, 7.6 and 7.0 ppm, respectively. The chemical shift anisotropies δ_σ determined by the Herzfeld−Berger analysis of the MAS spectra acquired at low MAS spinning frequencies ranging between 500 Hz and 3 kHz are 16.0 ± 1.4 and 13.0 ± 3.0 ppm for the two compounds, respectively.

On the other hand, the paramagnetic europium-substituted compounds **3**−**7** exhibit a large manifold of spinning sidebands spanning a range of ca. 400 ppm for the monomeric and dimeric compounds **3**−**6**, and 600 ppm for the tetrameric complex **7**. The isotropic chemical shifts in the solid state are also generally larger than in the diamagnetic complexes with the exception of $Al(H_3O)\{Eu(H_2O)_2PW_{11}O_{34}\}\cdot 20H_2O$ (**3**) ($\delta_{iso} = 5.6$ ppm), and vary significantly (between 5.6 and 54.2 ppm in **4**−**7**) depending on the nature of the Keggin solid. We note that the most likely reason for the low isotropic chemical shift in **3** is that it was

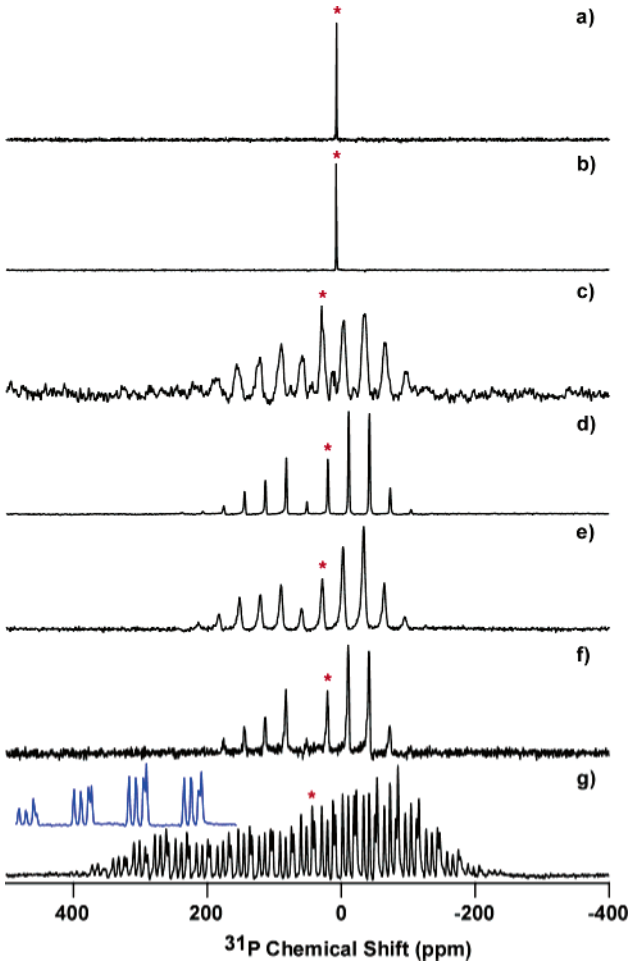

Figure 4. Experimental 9.4 T ^{31}P MAS NMR spectra of diamagnetic vanadium- substituted Keggin solids: (a) $K_4PVW_{11}O_{40}$ (**1**), (b) 1,2-$K_5[PV_2W_{10}O_{40}]$ (**2**), and europium-substituted Keggin compounds (c) $Al(H_3O)\{Eu(H_2O)_2PW_{11}O_{34}\}\cdot 20H_2O$ (**3**), (d) $K[Eu(PW_{11}O_{40})_2]^{13-}$ (**4**), (e) $Li_4[Eu(H_2O)_2PW_{11}O_{34}]$ (**5**), (f) Cs_{11} $Eu(PW_{11}O_{34})_2\cdot 28H_2O$ (**6**), and (g) $(NH_4)_{22}\{(Eu_2PW_{10}O_{38})_4(W_3O_8(H_2O)_2(OH)_4)\}\cdot 44H_2O$ (**7**) acquired at a spinning frequency of 5 kHz. The centerband is indicated with an asterisk. The isotropic chemical shifts are compiled in Table 1 with respect to 85% H_3PO_4. Compounds **3** and **5** represent a monomeric form of Keggin anion, while **4** and **6** are dimeric, as illustrated in Figures 1 and 2, respectively. Compound **7** is a tetramer. The inset in spectra g depicts that as expected, four crystallographically nonequivalent sites in the tetrameric **7** (shown in Figure 3) give rise to different isotropic chemical shifts.

prepared from a pH between 2 and 3, while compounds **4**−**7** were isolated at pH between 7 and 9. It has been demonstrated in several reports that ^{31}P solution chemical shifts of polyoxoanions are sensitive to pH.[47,48] The pH of the starting solution dictates the proton locations in the crystal lattice of the corresponding solid. Occluded protons in POM solids have been reported to impact significantly the ^{31}P chemical shifts in their solid-state NMR spectra.[49−51] The structure and chemistry of **3** suggests that the hydronium ion is within the crystal lattice, which is not the case for the other crystallized compounds **6** and **7** that are prepared under basic conditions and do not have protons occluded in their crystal lattices.

As described in the Experimental Section, the anisotropic spinning sideband envelopes are due to the large electron−nuclear dipolar interaction, dominating the spectra. As will be discussed in the subsequent sections of the manuscript, the contribution of the ^{31}P CSA is very small compared to the anisotropic electron−nuclear dipolar interaction and can therefore be neglected in the data analysis to a good approximation. Furthermore, the ^{31}P−^{183}W heteronuclear dipolar couplings are of the order of 46 Hz for the closest P−W distance (of 3.51 Å) and can therefore be also neglected. Similarly, the intermolecular homonuclear ^{31}P−^{31}P dipolar couplings are very weak, of the order of 25−28.5 Hz for the closest P−P pair in the tetramer (distance of 9.22 Å) and that in the dimer (distance of 8.83 Å). The natural abundance of ^{17}O is 0.2%, and therefore the ^{31}P−^{17}O dipolar coupling can also be disregarded to a very good approximation.

The electron−nuclear dipolar interaction is determined by the effective magnetic moments and by the geometry of the paramagnetic centers relative to the ^{31}P nucleus. For a single europium−phosphorus pair, the magnitude of the interaction is proportional to the inverse of the cube of the electron−nuclear distance (eq 5). When multiple europium sites are in close proximity to the phosphorus atom, the electron−nuclear dipolar interactions from the individual Eu−^{31}P pairs are added vectorially, as shown in eq 6. This is the case for the tetrameric compound **7** (Figures 3 and 4g), where the eight Eu atoms contribute strongly to the electron−nuclear dipolar interactions with each of the four crystallographically inequivalent phosphorus atoms, giving rise to the substantially stronger combined electron−nuclear interactions and correspondingly a larger breadth of the spinning sideband envelope.

As expected for the tetrameric compound **7**, the four crystallographically inequivalent P atoms yield different isotropic chemical shifts (see the inset to Figure 4g). Tentative assignment of the individual peaks belonging to the four P atoms (P1−P4) was made on the basis of the comparison between the experimental and the calculated electron−nuclear dipolar coupling tensors, as described below.

^{31}P Relaxation Parameters in Keggin Solids. We have determined the spin−lattice and spin−spin relaxation times for compounds **1**−**2** and **4**−**7** (summarized in Table 1).

As expected, the presence of paramagnetic center(s) in compounds **4**−**7** has a major effect on the relaxation parameters presented in Table 1, resulting in a decrease of T_1 by an order of magnitude (from ca. 22.9−35.9 s to 1.7−3.5 s), and of T_2 by a factor of ca. 2−10 (from 0.132−0.045 s to 0.016−0.027 s) with respect to those in diamagnetic solids **1** and **2**. Interestingly, the stoichiometry of the ion and the nature of the counterions introduce additional smaller yet significant variation to the relaxation parameters: T_1 varies within the range of 1.7−3.5 s and T_2 varies within the range of 0.016−0.027 s in **4**−**7**. We therefore conclude that relaxation rate constants are affected both by paramagnetic centers and (to a lesser but noticeable extent) by the anion stoichiometry and the nature of the counterions. The tetrameric solid **7** shows the fastest spin−lattice relaxation (T_1 of 1.66 s). Additional work is needed to examine whether the variations in T_1 are due to the countercations alone or are a much more complex function of the nature of the counterion, the crystal lattice parameters, and/or the hydration level of the compound. To this end we conclude that the ^{31}P relaxation parameters alone are not sufficient for deriving site-specific structural information.

Calculations of the Paramagnetic Dipolar Coupling in Crystallographically Characterized Keggin Solids. Compounds $Al(H_3O)\{Eu(H_2O)_2PW_{11}O_{34}\}\cdot 20H_2O$ (**3**), $Cs_{11}[Eu(PW_{11}O_{34})_2]\cdot 28H_2O$ (**6**), and $(NH_4)_{22}[(Eu_2PW_{10}O_{38})_4(W_3O_8(H_2O)_2(OH)_4)]\cdot 44H_2O$ (**7**) have been crystallographically characterized.[30] Compound **3** forms a 1:1 Eu/($PW_{11}O_{39}$) (monomeric) complex, **6** exists as a 1:2 Eu/($PW_{11}O_{39}$) (dimeric) solid, while **7** is a Eu-8 oxo/hydroxo cluster, where the four crystal-

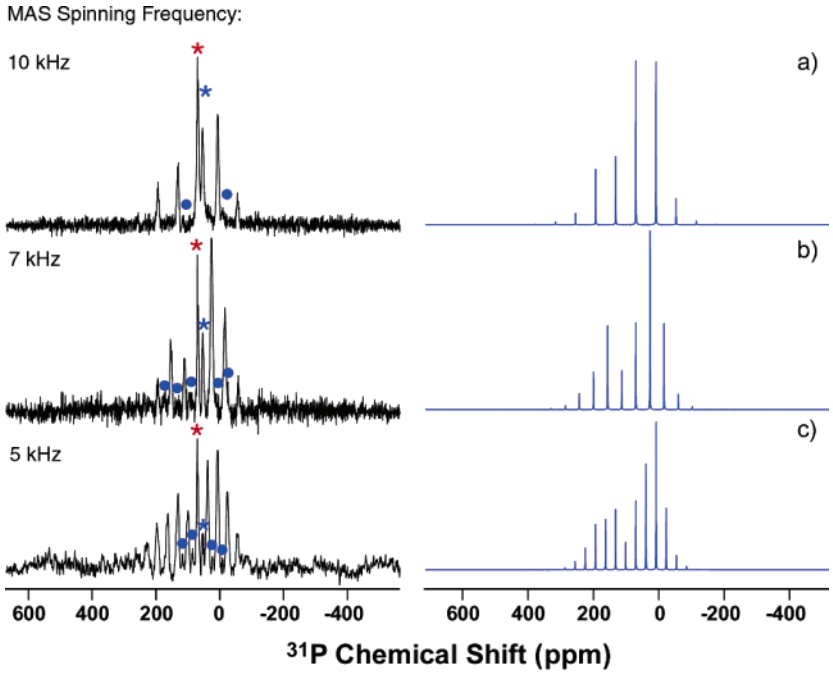

Figure 5. Experimental (black) and calculated (blue) ^{31}P MAS NMR spectra of $Al(H_3O)\{Eu(H_2O)_2PW_{11}O_{34}\}\cdot 20H_2O$ (**3**) at different spinning frequencies: (a) 10 kHz, (b) 7 kHz, and (c) 5 kHz. The isotropic spinning sideband of **3** is labeled with a red asterisk, the isotropic peak corresponding to the impurity is labeled with a blue asterisk, and the sideband manifold corresponding to the impurity is marked with blue circles.

TABLE 2: Calculated Electronic-Nuclear Dipolar Interaction for ^{31}P in Crystallographically Characterized Europium-Substituted Keggin Oxotungstates 3, 6, and 7[a]

	distance cutoff									
	single P−Eu pair or single P−Eu cluster in the tetrameric solid **7**[b]		15 Å		35 Å		60 Å		100 Å	
compd	Δδ, ppm	η	Δδ, ppm	η	Δδ, ppm	η	Δδ, ppm	η	Δδ, ppm	η
3	177.5	0	158.2	0.24	163.1	0.25	164.0	0.23	164.0	0.24
6	P1: 166.4	P1: 0	P1: 155.1	P1: 0.03	P1: 159.1	P1: 0.01	P1: 159.4	P1: 0.01	P1: 159.1	P1: 0.01
	P2: 170.6	P2: 0	P2: 161.6	P2: 0.07	P2: 163.7	P2: 0.07	P2: 163.8	P2: 0.06	P2: 163.7	P2: 0.06
7	P1: 307.8	P1: 0.43	P1: 319.7	P1: 0.48	P1: 315.4	P1: 0.48	P1: 317.7	P1: 0.48	P1: 318.2	P1: 0.48
	P2: 310.3	P2: 0.43	P2: 319.3	P2: 0.50	P2: 311.3	P2: 0.49	P2: 312.7	P2: 0.49	P2: 312.3	P2: 0.49
	P3: 267.5	P3: 0.75	P3: 282.4	P3: 0.38	P3: 279.6	P3: 0.42	P3: 281.7	P3: 0.41	P3: 282.3	P3: 0.41
	P4: 271.6	P4: 0.70	P4: 284.5	P4: 0.79	P4: 276.4	P4: 0.79	P4: 277.5	P4: 0.80	P4: 277.0	P4: 0.80

[a] Data are shown for $Al(H_3O)\{Eu(H_2O)_2PW_{11}O_{34}\}\cdot 20H_2O$ (**3**), $Cs_{11}[Eu(PW_{11}O_{34})_2]\cdot 28H_2O$ (**6**) and $(NH_4)_{22}[(Eu_2PW_{10}O_{38})_4(W_3O_8(H_2O)_2(OH)_4)]\cdot 44H_2O$ (**7**). Single Eu^{3+} ion and paramagnetic centers within 15, 35, 60, and 100 Å were included in the calculations. [b] For each of the four crystallographically inequivalent P atoms, individual interactions with eight europium atoms of the tetrameric cluster were summed up.

lographically inequivalent phosphorus atoms contain eight europium atoms within the range of 4.31−10.28 Å, corresponding to the individual dipolar interactions at 9.4 T ranging between 67.4 and 4.9 kHz, respectively. The coordination environments and the unit cells for these compounds are depicted in Figures 1−3.

For the ^{31}P solid-state NMR measurements, a fresh sample of the monomeric $Al(H_3O)\{Eu(H_2O)_2PW_{11}O_{34}\}\cdot 20H_2O$ (**3**) was synthesized. ^{31}P solution NMR measurements indicated the presence of a single monomeric Keggin species, as judged by the isotropic ^{31}P chemical shifts that were consistent with our previous reports.[30] However, this sample did not yield diffraction quality crystals. Furthermore, the ^{31}P solid-state NMR spectra recorded at different MAS spinning frequencies illustrated in Figure 5, reveal the presence of two different species: one corresponding to the compound of interest (as judged by the solid-state isotropic chemical shift of 5.6 ppm, which is very close to the solution value) and another one with the chemical shift of −10.7 ppm, most likely corresponding to an impurity of the lacunary $PW_{11}O_{39}^{7-}$ (Figure 5). Integrating the spectrum acquired at the MAS spinning frequency of 10 kHz indicates that the impurity is present at the level of ca. 10%. Both the main compound and the impurity are paramagnetic based on the fact that both give rise to a large manifold of spinning sidebands. The species with the isotropic shift of 5.6 ppm is characterized by the magnitude of the electron−nuclear dipolar coupling interaction of 161.5 ± 4.4 ppm, which is in close agreement with that expected on the basis of the geometry of this compound. On the other hand, for the impurity species, the electron−nuclear dipolar anisotropy is estimated to be 56.9 ± 7.2 ppm, which is not consistent with any of the Keggin solids where europium is part of the anion core. This relatively small electron−nuclear dipolar anisotropy compared to the other Eu Keggin solids probably reflects the large distance of the phosphorus of the lacunary $PW_{11}O_{39}^{7-}$ to a Eu of a nearby monomeric Keggin anion. We note that its presence does not interfere with the analysis of the spectra belonging to the main Keggin species of interest. We speculate that the presence of the impurity species explains why diffraction quality crystals could not be grown from this batch of sample. The sole

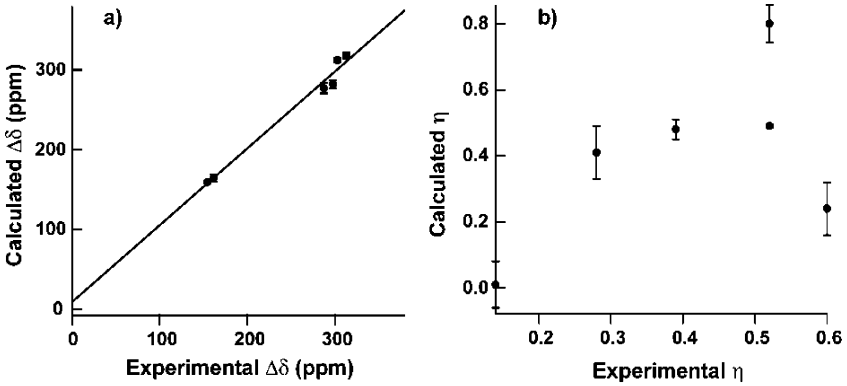

Figure 6. Comparison of experimental and calculated anisotropic NMR observables $\Delta\delta$ (a) and η (b) for crystallographically characterized compounds **3**, **6**, and **7**. For $\Delta\delta$, linear correlation between the experimental and calculated parameters was observed: $\Delta\delta_{calc} = 8.69 + 0.96\ \Delta\delta_{exp}$.

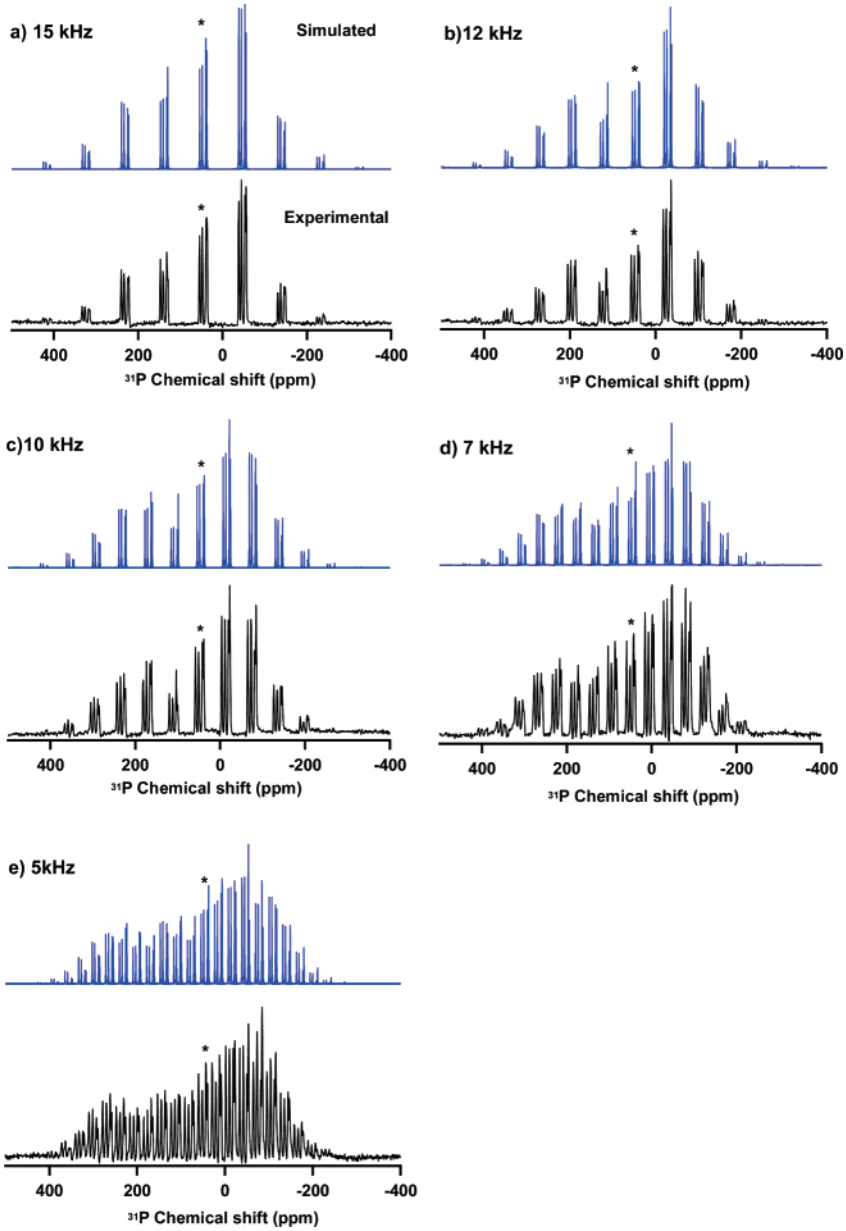

Figure 7. Experimental (black) and calculated (blue) ^{31}P MAS NMR spectra of tetrameric $(NH_4)_{22}\{(Eu_2PW_{10}O_{38})_4(W_3O_8(H_2O)_2(OH)_4)\}\cdot 44H_2O$ (**7**) at different spinning frequencies: (a) 15 kHz, (b) 12 kHz, (c) 10 kHz, (d) 7 kHz, and (e) 5 kHz. The four sets of spinning sidebands correspond to the four crystallographically nonequivalent sites. The spectral calculations were performed in SIMPSON using the combined electron−nuclear dipolar tensors computed from the X-ray crystallographic coordinates of the tetrameric compound **7**.

consequence of the presence of this impurity appears to be the formation of noncrystalline **3** having a heterogeneous distribution of isotropic chemical shifts, and we therefore proceed with the analysis of the data for this sample.

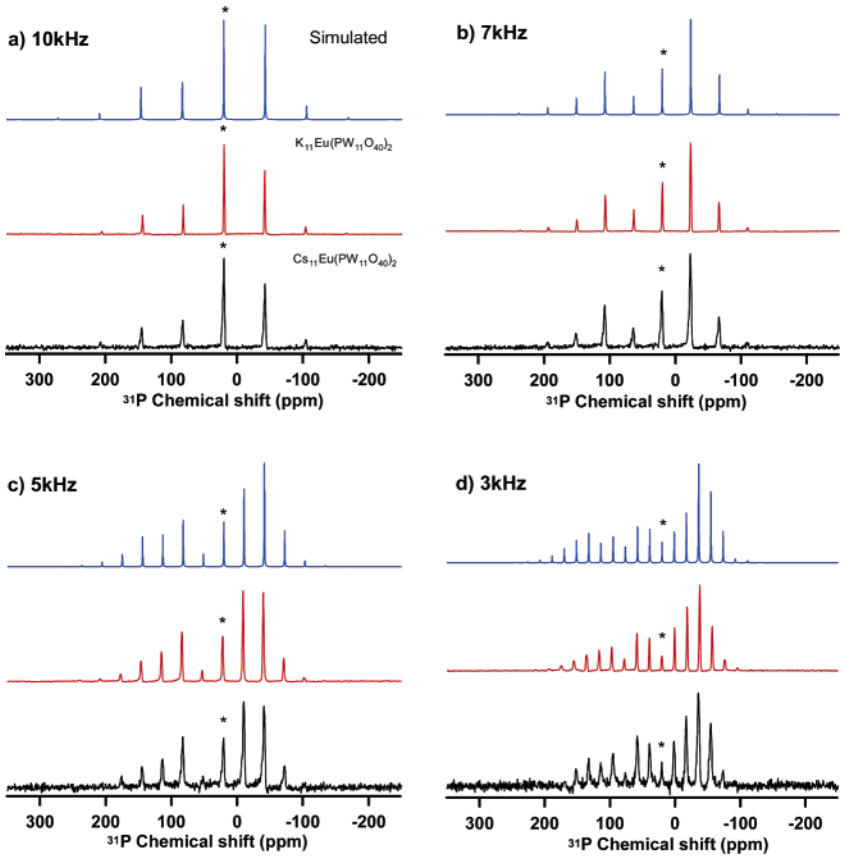

Figure 8. Experimental and calculated ^{31}P MAS NMR spectra of $K[Eu(PW_{11}O_{39})_2]^{13-}$ (**4**) and $Cs_{11}Eu(PW_{11}O_{34})_2 \cdot 28H_2O$ (**6**), at different spinning frequencies: (a) 10 kHz, (b) 7 kHz, (c) 5 kHz, and (d) 3 kHz. The experimental spectra for **4** and **6** are shown in red and black, respectively. The simulated spectra are in blue. The spectral calculations were performed in SIMPSON using the combined electron−nuclear dipolar tensors computed from the X-ray crystallographic coordinates for the dimeric compound **6**.

In Table 2, the Eu−^{31}P electron−nuclear dipolar interactions computed based on the experimental X-ray coordinates, are presented. The electron−nuclear dipolar matrices were calculated by first considering only those europium atoms that are within a single Keggin anion cluster (monomeric, dimeric, or tetrameric), and then subsequently including additional Eu sites that are within 15, 35, 60, and 100 Å from the phosphorus atom. For the monomeric and dimeric species, the calculations converge at 35 Å. For the tetrameric species, it is necessary to consider the europium sites within 60 Å, because of the stronger overall electron−nuclear interaction and the complex relative geometries of the individual Eu−P pairs. For comparison, Brough, Grey, and Dobson previously observed that including europium atoms up to 100 Å was necessary to reach convergence in the calculations of the ^{13}C of rare earth acetates.[25] The most likely reason for the faster convergence in the Keggin compounds is the larger size of the anionic cluster, and the larger crystallographic unit cell, compared to the acetate salts.

We note that the overall agreement between the experimental and the calculated values of the electron−nuclear dipolar anisotropy is very good, within 1.5−6% at all MAS frequencies (Tables 2, 3, and Figure 6), confirming that this is the dominant interaction in the paramagnetic europium-substituted Keggin solids, and that the contribution from the ^{31}P chemical shift anisotropy is very small and can be disregarded in the data analysis to a good approximation. The agreement between the experimental and the calculated asymmetry parameters of the combined electron−nuclear dipolar tensor is somewhat worse, especially for the monomeric $Al(H_3O)\{Eu(H_2O)_2PW_{11}O_{34}\}\cdot 20H_2O$ (**3**). Closer inspection of the ^{31}P MAS spectrum of this compound (Figure 4c) reveals that the individual spinning sidebands are much broader than for the rest of the paramagnetic compounds 4−7 (Figure 4d−g), suggesting an inhomogeneous distribution of isotropic chemical shifts due to the conformational heterogeneity is present in the sample. (Indeed, the batch of this compound utilized in the measurements did not yield diffraction quality crystals.) The maximum intensities of the individual peaks are therefore less well defined than in the crystalline compounds with narrow lines, resulting in the lower precision of the experimentally measured anisotropy parameter. We also note that a slight difference is expected in the Eu−P electron−nuclear dipolar interaction for the P1 and P2 atoms in the dimeric compound $Cs_{11}[Eu(PW_{11}O_{34})_2]\cdot 28H_2O$ (**6**) (Table 2). However, these two atoms have the same isotropic chemical shifts in solution and in the solid state and could not be distinguished.

In the tetrameric compound **7**, we assigned each of the isotropic chemical shifts to the four crystallographically inequivalent phosphorus atoms via the inspection of the experimental and calculated electron−nuclear anisotropy and asymmetry parameters. The assignment presented in Table 1 gives rise to the smallest possible discrepancies between the experiment and the calculations.

Figures 7−9 illustrate the overall good agreement between the experimental spectra and those calculated based on the electron−nuclear dipolar interaction parameters generated using the X-ray coordinates, for the tetramer **7**, the dimeric compounds **4** and **6**, and the monomeric solid **5**.

Electron−Nuclear Dipolar Coupling as a Structural Probe in Keggin Solids. As discussed above, the analysis of the known

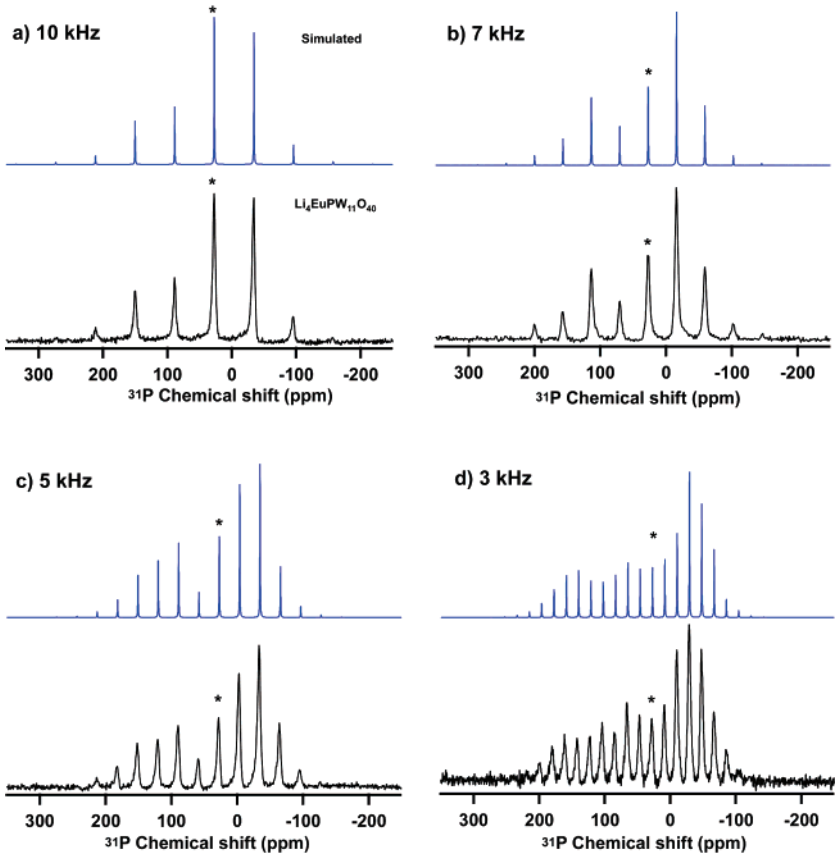

Figure 9. Experimental (black) and calculated (blue) ^{31}P MAS NMR spectra of $Li_4[Eu(H_2O)_2PW_{11}O_{34}]$ (**5**) at different spinning frequencies: (a) 10 kHz, (b) 7 kHz, (c) 5 kHz, and (d) 3 kHz. The spectral calculations were performed in SIMPSON using the combined electron−nuclear dipolar tensors computed from the X-ray crystallographic coordinates for the monomeric compound **3**.

X-ray coordinates yields the calculated Eu−^{31}P electron−nuclear dipolar interactions for different Keggin solids, which are in close agreement with the experimental ^{31}P solid-state NMR results. However, to be a useful structural probe, the ^{31}P MAS NMR measurements should yield distance and/or geometry information in the absence of any crystallographic information. This is especially critical for analysis of polyoxometalates that are inherently amorphous or for which diffraction quality crystals cannot be easily obtained, such as thin films.

To date, only three types of species have been observed in europium-substituted Keggin solids: 1:1 (monomeric), 1:2 (dimeric), and Eu-8 oxo/hydroxo clusters.[30] As is clear from Table 1, each species gives rise to a distinct set of ^{31}P NMR parameters: the isotropic chemical shifts, the anisotropy and asymmetry of the electron−nuclear dipolar interaction. Therefore, it appears that these NMR observables could potentially be used as a qualitative probe of the speciation of the Keggin molecule. For example, the tetrameric species can be immediately distinguished by their large electron−nuclear dipolar anisotropies, high asymmetry parameters, and isotropic chemical shifts above 37.3 ppm.

Furthermore, comparison of the anisotropic NMR parameters for $K[Eu(PW_{11}O_{39})_2]^{13-}$ (**4**) and $Li_4[Eu(H_2O)_2PW_{11}O_{34}]$ (**5**) with those of compounds **3** and **6**, suggests that **4** is expected to be dimeric, while **5** is expected to be monomeric. We do not have X-ray crystallographic information for these two solids. However, as was discussed in the preceding sections, our prior work indicates that formation of a 1:2 dimeric species is generally observed when Cs^+ and K^+ are used as countercations, while 1:1 monomeric species are generated with Al^{3+} and Li^+ counterions,[30,42,43] which is in agreement with our solid-state NMR results discussed herein. Moreover, upon subsequent dissolution of these solids in water, the ^{31}P NMR solution spectra reveal clearly the 1:1 and 1:2 species for compounds **5** and **4**, respectively.[30]

Additionally, we have examined whether reliable P−Eu distance estimates can be obtained in the monomeric and dimeric Keggin solids by making a single electron−nuclear spin−pair approximation. Presented in Table 4 for the monomeric **3** and dimeric **6** compounds, are ranges of the electron−nuclear dipolar anisotropy and the corresponding distances based on a single spin-pair approximation. The experimental X-ray distances for **3** and **6** are 4.390 and 4.486 Å, which would correspond to the electron−nuclear dipolar anisotropy $\Delta\delta$ of 177.5 and 166.4 ppm, respectively. The experimentally measured values of $\Delta\delta$ for **3** and **6** are 170.7 and 154.0 ppm, which yield the distances of 4.447 and 4.603 Å, respectively. Thus the discrepancies between the experimental and the estimated distances are 0.057 and 0.117 Å, respectively, which is a very good agreement for the Keggin molecules and for polyoxometalate solids in general. We note that, however, the single electron−nuclear spin-pair approximation is not valid in the tetrameric compound **7**, where eight europium sites are in close proximity and make large individual contributions to the combined dipolar coupling tensor.

We also note that isotropic ^{31}P chemical shifts alone do not always provide unambiguous information about the geometric and electronic structure of Keggin solids. For example, the isotropic chemical shift of $Al(H_3O)\{Eu(H_2O)_2PW_{11}O_{34}\}\cdot 20H_2O$ (**3**) is 5.6 ppm, which differs only slightly from the shifts of the diamagnetic complexes **1** and **2**. However, this compound is clearly paramagnetic based on our previous work,[30] and on the large electron−nuclear dipolar anisotropies detected in the

TABLE 3: Experimental ^{31}P Electron−Nuclear Dipolar Anisotropies ($\Delta\delta$, η) for Different Spinning Frequencies[a]

		$\Delta\delta$, ppm[b]				η[b]			
compd	MAS spinning frequency, Hz	P1	P2	P3	P4	P1	P2	P3	P4
3	5000	160.2				0.76			
	6930	169.7				0.52			
	10052	154.6				0.52			
		161.5 ± 4.4				0.6 ± 0.08			
4	2103	152.8				0.09			
	3112	153.25				0.17			
	5030	155.05				0.14			
	6991	154.05				0.03			
	9985	149.95				0.15			
		153.0 ± 0.9				0.12 ± 0.03			
5	3045	171.1				0.28			
	5018	175.1				0.25			
	7000	166.3				0.34			
	9972	170.3				0.00			
		170.7 ± 1.8				0.22 ± 0.15			
6	3036	156.3				0.24			
	5012	153.2				0.27			
	7062	151.6				0.00			
	10192	154.9				0.04			
		154 ± 1.0				0.14 ± 0.07			
7	5027	323.2	305.8	310.9	294.4	0.37	0.52	0.34	0.34
	7014	317.0	299.0	307.7	307.3	0.40	0.53	0.42	0.61
	9960	310.7	312.0	298.2	285.2	0.45	0.50	0.44	0.44
	12032	314.0	301.1	289.5	270.8	0.44	0.51	0.21	0.64
	15018	300.7	296.0	283.4	279.3	0.28	0.53	0.00	0.58
		313.1 ± 3.7	302.8 ± 2.8	297.9 ± 5.2	287.4 ± 6.3	0.39 ± 0.03	0.52 ± 0.006	0.28 ± 0.08	0.52 ± 0.057

[a] Data are shown for $Al(H_3O)\{Eu(H_2O)_2PW_{11}O_{34}\}\cdot 20H_2O$ (**3**), $K[EuPW_{11}O_{40}]^{13-}$ (**4**), $Li_4[Eu(H_2O)_2PW_{11}O_{34}]$ (**5**), $Cs_{11}[Eu(PW_{11}O_{34})_2]\cdot 28H_2O$ (**6**), and $(NH_4)_{22}[(Eu_2PW_{10}O_{38})_4(W_3O_8(H_2O)_2(OH)_4)]\cdot 44H_2O$ (**7**). The chemical shift anisotropy is very small and can be neglected to a good approximation. [b] The last line reports the mean value and the standard error.

TABLE 4: Calculated Electron−Nuclear Dipolar Anisotropies and Corresponding P−Eu Distances for Monomeric and Dimeric Keggin Solids Assuming A Single P−Eu Pair[a]

compound	P−Eu distances (Å)	$\Delta\delta$, ppm
3	4.190	204.1
	4.291	190.2
	4.390[b]	177.5
	4.447	170.7[c]
	4.490	165.9
	4.591	155.2
	4.690	145.6
6	4.185	204.9
	4.285	190.9
	4.385	178.6
	4.486[b]	166.4
	4.586	155.8
	4.603	154.0[c]
	4.682	146.3

[a] Data are shown for $Al(H_3O)\{Eu(H_2O)_2PW_{11}O_{34}\}\cdot 20H_2O$ (**3**) and $Cs_{11}[Eu(PW_{11}O_{34})_2]\cdot 28H_2O$ (**6**). [b] P−Eu distances from X-ray structures [c] Experimentally observed dipolar anisotropy.

MAS spectra reported here (vide supra). The isotropic shifts in paramagnetic compounds are a complex function of the nucleus' environment beyond the first coordination sphere and of pH, and large chemical shift variations in paramagnetic systems are commonly observed. There are no empirical relationships established for the paramagnetic Keggin solids under investigation that would permit correlating the experimentally recorded isotropic chemical shifts with the structure of the solid. Therefore, to gain thorough understanding of the electronic structure and the isotropic chemical shifts in the paramagnetic Keggin solids under investigation, high-level quantum mechanical calculations are required. These are beyond the scope of the current study. On the other hand, the electron−nuclear dipolar interaction is a direct structural probe and depends only on the effective magnetic moment, the geometry, and the distances between the nucleus and the paramagnetic sites. Our results therefore reinforce the importance of determination of anisotropic electron−nuclear dipolar interaction by solid-state NMR.

Conclusions

^{31}P MAS NMR spinning sideband envelopes in europium-substituted Keggin solids are dominated by the electron−nuclear dipolar interaction. The anisotropy and the asymmetry parameters corresponding to the electron−nuclear dipolar coupling tensor report on the geometry of the paramagnetic europium centers, and on the speciation of the Keggin solids. In the absence of X-ray crystallographic information, P−Eu distance estimates accurate to within 0.06−0.12 Å can be extracted directly from the magnitude of the electron−nuclear dipolar coupling using the single electron−nuclear spin−pair approximation. ^{31}P MAS NMR spectroscopy is expected to be generally applicable for structural analysis of paramagnetic Keggin solids, and especially useful in the absence of a long-range order.

Acknowledgment. T.P. acknowledges financial support of the University of Delaware, of the National Science Foundation (NSF-CAREER Grant CHE-0237612) and the National Institutes of Health (Grant P20-17716, COBRE individual subproject). T.P. and B.G. acknowledge the financial support of the ACS Petroleum Research Fund (PRF Grant No. 39827-G5M and the 2004 SRF supplement). L.C.F. acknowledges financial support of the National Science Foundation (NSF Grant No.

CHE 0414218), of the National Institutes of Health (NIH-S06 GM60654 (SCORE)), and NSF Grant MRI0116244 for the purchase of an X-ray diffractometer. Research infrastructure at Hunter College is partially supported by NIH-Research Centers in Minority Institutions Grant RR03037-08.

References and Notes

(1) Wassermann, K.; Palm, R.; Lunk, H.; Fuchs, J.; Steinfeldt, N.; Stosser, R. *Inorg. Chem.* **1995**, *34*, 5029−5036.
(2) Katsoulis, D. E. *Chem. Rev.* **1998**, *98*, 359−387.
(3) Pope, M. T.; Müller, A. *Angew. Chem., Int. Ed. Engl.* **1991**, *30* (1), 34−48.
(4) Berzelius, J. J. *Poggendorffs Ann. Phys. Chem.* **1826**, *6*, 369−380.
(5) Keggin, J. F. *Nature (London)* **1933**, *131*, 908.
(6) Kortz, U.; Mbomekalle, I. M.; Keita, B.; Nadjo, L.; Berthet, P. *Inorg. Chem.* **2002**, *41* (24), 6412−6416.
(7) Coronado, E.; Gómez-García, C. J. *Chem. Rev.* **1998**, *98*, 273−296.
(8) Bekiari, V.; Lianos, P. *Adv. Mater.* **1998**, *10* (17), 1455−1458.
(9) Buonocore, G. E.; Li, H.; Marciniak, B. *Coord. Chem. Rev.* **1990**, *99*, 55−87.
(10) Yamase, T. *Chem. Rev.* **1998**, *98* (1), 307−325.
(11) Ma, H. Y.; Peng, J.; Han, Z. G.; Feng, Y. H.; Wang, E. *Thin Solid Films* **2004**, *446* (2), 161−166.
(12) Wang, J.; Liu, F. Y.; Fu, L. S.; Zhang, H. J. *Mater. Lett.* **2002**, *56* (3), 300−304.
(13) Wang, X. L.; Wang, Y. H.; Hu, C. W.; Wang, E. B. *Mater. Lett.* **2002**, *56* (3), 305−311.
(14) Jiang, M.; Zhang, H.; Wang, E. B.; Kang, Z. H.; Lian, S. Y.; Xu, L.; Wu, A. G.; Li, Z. *Chem. Res. Chin. Univ.* **2004**, *20* (1), 15−19.
(15) Wang, Y. H.; Wang, X. L.; Hu, C. W.; Wang, E. B.; Shi, C. S. *Chin. J. Chem.* **2002**, *20* (4), 336−340.
(16) Ma, H. Y.; Peng, J.; Zhou, B. B.; Han, Z. G.; Feng, Y. H. *Appl. Surf. Sci.* **2004**, *233* (1−4), 14−19.
(17) Wang, Z.; Wang, J.; Zhang, H. J. *Mater. Chem. Phys.* **2004**, *87* (1), 44−48.
(18) Wang, J.; Wang, Z.; Wang, H. S.; Liu, F. Y.; Fu, L. H.; Zhang, H. J. *J. Alloys. Compd.* **2004**, *376* (1−2), 68−72.
(19) Yamase, T.; Sugeta, M. *J. Chem. Soc., Dalton Trans.* **1993**, (5), 759−765.
(20) Yamase, T.; Kobayashi, T.; Sugeta, M.; Naruke, H. *J. Phys. Chem. A* **1997**, *101* (28), 5046−5053.
(21) Lee, Y. J.; Grey, C. P. *J. Phys. Chem. B* **2002**, *106* (14), 3576−3582.
(22) Nayeem, A.; Yesinowski, J. P. *J. Chem. Phys.* **1988**, *89* (8), 4600−4608.
(23) Lee, H.; Polenova, T.; Beer, R. H.; McDermott, A. E. *J. Am. Chem. Soc.* **1999**, *121* (29), 6884−6894.
(24) Liu, K.; Ryan, D.; Nakanishi, K.; Mcdermott, A. *J. Am. Chem. Soc.* **1995**, *117* (26), 6897−6906.
(25) Brough, A. R.; Grey, C. P.; Dobson, C. M. *J. Am. Chem. Soc.* **1993**, *115* (16), 7318−7327.
(26) Tucker, M. C.; Doeff, M. M.; Richardson, T. J.; Finones, R.; Reimer, J. A.; Cairns, E. J. *Electrochem. Solid State* **2002**, *5* (5), A95-A98.
(27) Woehler, S. E.; Wittebort, R. J.; Oh, S. M.; Hendrickson, D. N.; Inniss, D.; Strouse, C. E. *J. Am. Chem. Soc.* **1986**, *108* (11), 2938−2946.
(28) Brough, A. R.; Grey, C. P.; Dobson, C. M. *J. Chem. Soc. Chem. Commun.* **1992**, (10), 742−743.
(29) Lin, T. H.; Dinatale, J. A.; Vold, R. R. *J. Am. Chem. Soc.* **1994**, *116* (5), 2133−2134.
(30) Zhang, C.; Howell, R. C.; Scotland, K. B.; Perez, F. G.; Todaro, L.; Francesconi, L. C. *Inorg. Chem.* **2004**, *43* (24), 7691−7701.
(31) Domaille, P. J. *J. Am. Chem. Soc.* **1984**, *106*, 7677−7687.
(32) Huang, W. L.; Todaro, L.; Yap, G. P. A.; Beer, R.; Francesconi, L. C.; Polenova, T. *J. Am. Chem. Soc.* **2004**, *126* (37), 11564−11573.
(33) Vold, R. L.; Waugh, J. S.; Klein, M. P.; Phelps, D. E. *J. Chem. Phys.* **1968**, *48* (8), 3831−3832.
(34) Meiboom, S.; Gill, D. *Rev. Sci. Instrum.* **1958**, *29* (8), 688−691.
(35) Cobas, J.; Cruces, J.; Sardina, F. J. *Mestre-C: Magnetic Resonance Companion*; Departmento de Quimica Organica, Facultat de Quimica: Universidad de Santiago de Compostela, Spain, 2000.
(36) Selwood, P. W. Atomic Diamagnetism. In *Magnetochemistry*, 2nd ed.; Interscience Publishers: New York, 1956; Vol. 1, pp 69−82.
(37) Bak, M.; Rasmussen, J. T.; Nielsen, N. C. *J. Magn. Reson.* **2000**, *147*, 296−330.
(38) Herzfeld, J.; Berger, A. E. *J. Chem. Phys.* **1980**, *73* (12), 6021−6030.
(39) Eichele, K.; Wasylishen, R. E. *Herzfeld-Berger Analysis Program*, version 1.4.4; Dalhousie University, Halifax, Canada, 2001.
(40) Abragam, A.; Bleaney, B. *Electron Paramagnetic Resonance of Transition Ions*, 1st ed.; Clarendon Press: Oxford, 1970; Vol. 1, p 911.
(41) Maricq, M. M.; Waugh, J. S. *J. Chem. Phys.* **1979**, *70* (7), 3300−3316.
(42) Zhang, C.; Howell, R. C.; Luo, Q. H.; Fieselmann, H. L.; Todaro, L. J.; Francesconi, L. C. *Inorg. Chem.* **2005**, *44* (10), 3569−3578.
(43) Zhang, C.; Bensaid, L.; McGregor, D.; Fang, S.; Howell, R. C.; Burton-Pye, B.; Luo, Q.; Todaro, L.; Francesconi, L. C. *J. Cluster Sci.*, in press.
(44) Selwood, P. W. *J. Am. Chem. Soc.* **1933**, *55*, 4869−4875.
(45) Hughes, G.; Pearce, D. W. *J. Am. Chem. Soc.* **1933**, *55*, 3277−3279.
(46) Frank, A. *Phys. Rev.* **1935**, *48*, 765−771.
(47) Selling, A.; Andersson, I.; Grate, J. H.; Pettersson, L. *Eur. J. Inorg. Chem.* **2000**, (7), 1509−1521.
(48) Pettersson, L.; Andersson, I.; Selling, A.; Grate, J. H. *Inorg. Chem.* **1994**, *33* (5), 982−993.
(49) Ganapathy, S.; Fournier, M.; Paul, J. F.; Delevoye, L.; Guelton, M.; Amoureux, J. P. *J. Am. Chem. Soc.* **2002**, *124* (26), 7821−7828.
(50) Essayem, N.; Tong, Y. Y.; Jobic, H.; Vedrine, J. C. *Appl. Catal., A* **2000**, *194*, 109−122.
(51) Essayem, N.; Coudurier, G.; Fournier, M.; Vedrine, J. C. *Catal Lett.* **1995**, *34* (1−2), 223−235.